Glutamate Transport Proteins and Metabolic Enzymes are Poor Prognostic Factors in Invasive Lobular Carcinoma

Todd A. Young[1], Shaymaa Bahnassy[1], Theresa C. Abalum[1,2], Eden A. Pope[1,3], Amanda Torres Rivera[1], Aileen I. Fernandez[1,4], Ayodeji O. Olukoya[1], Dua Mobin[1], Suman Ranjit[5], Nicole E. Libbey[1], Sonali Persaud[1], Aaron M. Rozeboom[1], Krysta Chaldekas[1], Brent T. Harris[1,6], Zeynep Madak-Erdogan[7], Joseph L. Sottnik[8], Matthew J. Sikora[8], Rebecca B. Riggins[1,9]

[1]Department of Oncology, Lombardi Comprehensive Cancer Center, Georgetown University, Washington, DC 20057
[2]Towson University, Towson, MD 21252
[3]Wake Forest University, Winston-Salem, NC 27109
[4]Department of Pathology, Yale School of Medicine, New Haven, CT 06520
[5]Department of Biochemistry and Molecular & Cellular Biology, Georgetown University Medical Center, Washington, DC 20057
[6]Departments of Neurology and Pathology, Georgetown University Medical Center, Washington, DC 20057
[7]Department of Food Science and Human Nutrition, Cancer Center at Illinois, Division of Nutritional Sciences, University of Illinois Urbana-Champaign, Urbana, IL 61801
[8]Department of Pathology, University of Colorado Anschutz Medical Campus, Aurora, CO 80045

[9]Corresponding author: Rebecca B. Riggins, PhD

Email: rbr7@georgetown.edu

Phone: 202 687 1260

Conflict of interest: Authors declare no conflict of interest.

Disclosures: AIF reported employment from Caris Life Sciences outside the submitted work. AMR reported employment from Leidos Biomedical Research outside the submitted work. KC reported employment from AstraZeneca outside the submitted work. RBR reported serving as an Associate Editor for the *Journal of the Endocrine Society* outside the submitted work. ZME reported serving as Editor in Chief of the *Journal of the Endocrine Society* outside the submitted work.

Running title: Glutamate transport and metabolism in ILC

Abstract

Invasive Lobular Carcinoma (ILC) is a subtype of breast cancer characterized by distinct biological features, and limited glucose uptake coupled with increased reliance on amino acid and lipid metabolism. Our prior studies highlight the importance of glutamate as a key regulator of ILC tumor growth and therapeutic response. Here we examine the expression of four key proteins involved in glutamate transport and metabolism – SLC3A2, SLC7A11, GPX4, and GLUD1/2 – in a racially diverse cohort of 72 estrogen receptor-positive (ER+) ILC and 50 ER+ invasive ductal carcinoma, no special type (IDC/NST) patients with primary disease. All four proteins are associated with increased tumor size in ILC, but not IDC/NST, with SLC3A2 also specifically linked to shorter overall survival and the presence of comorbidities in ILC. Notably, GLUD1/2 expression is associated with ER expression in ILC, and is most strongly associated with increased tumor size and stage in Black women with ILC from our cohort and TCGA. We further explore the effects of GLUD1 inhibition in endocrine therapy-resistant ILC cells using the small-molecule inhibitor R162, which reduces ER protein levels, increases reactive oxygen species, and inhibits oxidative phosphorylation. These findings highlight a potentially important role for glutamate metabolism in ILC, particularly for Black women, and position several of these glutamate-handling proteins as potential targets for therapeutic intervention in ILC.

Keywords

Invasive lobular carcinoma, glutamate metabolism, GPX4, GLUD1, disparities

Introduction

ILC (Invasive Lobular Carcinoma) is a special histological subtype of breast cancer that accounts for 10-15% of cases diagnosed annually[1,2] . ILC has unique genetic, transcriptomic, and biological features as compared to the more common invasive ductal breast cancer, or breast cancer of no special type (IDC/NST). Nearly all ILC is estrogen receptor-positive (ER+), and characterized by mutational inactivation of *CDH1*, the gene encoding E-cadherin[3], which is associated with the diffuse growth pattern of ILC tumors. Additionally, ILC metastasizes to the lung, bone, and brain like other ER+ breast malignancies, but it also has a propensity to spread to the digestive tract, ovaries, and the peritoneal cavity[1,2]. Complicating this atypical dissemination pattern, advanced or metastatic ILC may not be as easily detected by positron emission tomography using the glucose analog tracer ^{18}F-fluorodeoxyglucose (i.e. [^{18}F]FDG-PET)[4], as several clinical studies have shown ILC has limited FDG avidity. While these observations complicate care of patients with metastatic ILC, they also suggest that ILC has a distinct metabolic phenotype among breast cancers that is less reliant on glucose uptake and metabolism.

Other PET tracers provide opportunities to understand differential ILC metabolism. For example, fluciclovine is an amino acid analog of leucine[5] , and prospective clinical trials demonstrate that ILC shows substantially higher [^{18}F] Fluciclovine-PET uptake compared to [^{18}F]FDG-PET][6–8]. Among ILC, 100% of lesions were fluciclovine-positive while only 43% of lesions were FDG-positive. These findings are consistent with clinical and preclinical research, in which we and others show that ILC is more dependent on lipid and amino acid metabolism compared to glucose metabolism[9–12]. Our work suggests that the amino acid glutamate may be particularly important in ILC. Endocrine therapy-resistant ILC models upregulate multiple metabotropic glutamate receptors (mGluRs)[13], and the small molecule Riluzole (a modulator of glutamate metabolism FDA approved for amyotrophic lateral sclerosis) is efficacious against *in vitro, in vivo*, and *ex vivo* models of ILC[14,15], (discussed in[16]). Therefore, understanding glutamate metabolism in ILC can provide important opportunities to advance imaging and clinical management, as well as precision treatment paradigms.

For this study, we assembled a cohort of 72 ER+ primary ILCs and 50 ER+ primary IDC/NSTs with well-annotated clinical, pathological, and demographic data, and used multiplex immunohistochemistry (IHC) to determine the prognostic value of four key proteins in glutamate transport and metabolism (**Figure 1A**). Solute carriers 3A2 (SLC3A2 or CD98) and 7A11 (SLC7A11) heterodimerize to form System xCT, an antiporter that imports cystine and exports glutamate. Downstream of xCT, glutathione peroxidase 4 (GPX4) reduces the glutamate-glycine-cysteine tripeptide glutathione (GSH) to glutathione disulfide (GSSG) and inhibits ferroptosis, an iron-dependent mechanism of cell death. Finally, glutamate dehydrogenase 1/2 (GLUD1/2 or GDH1/2) is a bidirectional metabolic enzyme that in the forward direction converts glutamate to alpha-ketoglutarate to replenish the tricarboxylic acid (TCA) cycle, while in the reverse direction it recycles ammonia to bolster tumor cell growth and amino acid synthesis[17,18].

xCT promotes metastasis and therapy resistance in multiple cancers, including breast cancer[19]. As a negative regulator of ferroptosis downstream of xCT, GPX4 expression in cancer and stromal cells is also associated with disease progression and invasiveness[20–22]. GLUD1/2 has recently emerged as a key node connecting glutamate metabolism, xCT function, and ferroptosis[23–25]. However, the contribution of these proteins to ILC biology and prognosis is not known, despite mounting evidence highlighting the importance of glutamate metabolism in this breast cancer subtype.

Methods

Use and Re-Use of Publicly Available and Previously Published Data. mRNA expression data from invasive lobular breast cancer (ILC), mixed ductal-lobular breast cancer (mDLC), and breast cancer of no special type (NST) from The Cancer Genome Atlas (TCGA, RRID:SCR_003193) pan-cancer clinical data resource[26] , METABRIC[27] , and the Sweden Cancerome Analysis Network - Breast (SCAN-B)[28,29] shown in **Figure S1A** were accessed via Gene Expression eXPLORER (GEXPLORER) at https://leeoesterreich.org/resources on 6/4/2024. mRNA expression data and associated clinicopathological data from ILC and IDC/NST from TCGA shown in **Figure 4C** were accessed via cBioPortal[30,31] (RRID:SCR_014555) on 6/13/2024. Enrichr was used for gene set enrichment analysis[32–34]. GLUD1 peptide counts from ER rapid immunoprecipitation mass spectrometry of endogenous proteins (RIME) in ILC cell lines shown in **Figure 6A** were graphed from Supplemental File 6 of Sottnik et al[35] .

Cell Culture and Reagents. Cell lines were maintained at 37°C in a humidified incubator with 95% air and 5% carbon dioxide (CO_2). Cell lines were authenticated by short tandem repeat (STR) profiling, and regularly tested to ensure they remained free of *Mycoplasma spp*. contamination, by the Tissue Culture and Biobanking Shared Resource (TCBSR). The following ER+ ILC cell lines were cultured as previously described[14,36,37] : SUM44PE (RRID:CVCL_3424) and its tamoxifen-resistant derivative LCCTam; and MDA-MB-134VI (RRID:CVCL_0617) and its long-term estrogen-deprived (LTED) derivatives LTED-A, -B, -D, and -E. General cell culture supplements and reagents were purchased from ThermoFisher (Grand Island, NY) or Sigma Aldrich, St. Louis, MO). The glutamate dehydrogenase inhibitor R162 and reactive oxygen species (ROS) inducer tert-Butyl hydroperoxide (TBHP, positive control) were purchased from Sigma (Cat#s 538098 and 416665, respectively). Oligomycin A was purchased from Selleckchem (Houston, TX, Cat# S1478).

Immunoblotting. Assays were conducted as previously described[14] and whole-cell lysates were probed with the following primary antibodies: SLC3A2 (1:1000, Santa Cruz Biotechnology Cat# sc-376815, RRID:AB_2938854); SLC7A11 (1:500, Abcam Cat# ab175186, RRID: AB_2722749); GLUD1/2 (1:1000, Cell Signaling Technology Cat# 12793, RRID:AB_2750880); GPX4 (1:1000, Abcam Cat# ab125066, RRID: AB_10973901); ER alpha (clone D8H8; 1:1000, Cell Signaling Technology Cat# 8644, RRID:AB_2617128); and beta-actin (1:2000, Cell Signaling Technology Cat# 3700, RRID:AB_2242334).

CellROX ROS Assays. SUM44 and LCCTam cells were seeded in 6-well plates at 300,000 cells/well. Forty-eight hours later, cells were treated with DMSO or 10 μM R162 for 4 hours before collection and staining with CellROX Deep Red (ThermoFisher, Cat# C10422) and SYTOX Blue (ThermoFisher, Cat# S11348). Flow cytometric analysis was performed by the Flow Cytometry Shared Resource (FCSR).

Metabolic Imaging of NADH Autofluorescence, Fluorescent Lifetime Imaging (FLIM) Instrumentation, and Phasor Analysis. LCCTam cells were seeded on 22 mm^2 diameter glass coverslips (VWR, Radnor, PA, Cat# 48380-046) in 6-well plates at 150,000 cells/well. Forty-eight hours later, cells were treated with DMSO, 100 μM oligomycin, or 10 μM R162 for 12 hours before transferring coverslips to 35 mm^2 diameter glass bottom dishes (MatTek, Ashland, MA, Cat# P35GCOL-1.5-14-C) and performing live-cell imaging on the FVMPE-RS multi-photon, laser-scanning microscope (Olympus, Waltham, MA) with deep imaging via emission recovery (DIVER) detector in the Microscopy and Imaging Shared Resource (MISR). Cells were imaged using a 40X water objective (Olympus, Waltham, MA) using a 740 nm laser from an InsightX3 laser. The signal was collected using the DIVER detector in the forward direction that is connected to a

FastFLIM acquisition card (ISS, Champaign IL). The FLIM data acquisition and analysis was carried out using SimFCS (www.lfd.uci.edu). The fractional intensity of free NADH was calculated from the positions of free and bound NADH in the phasor representation of FLIM data as described previously[14,38–40] .

Primary Breast Cancer Cohorts and Tissue Microarray (TMA) Construction. The ER+ IDC/NST cohort and TMA construction has been previously described[41] . For the ILC cohort, we similarly constructed a TMA with ≥2 cores per patient from n=72 patients with primary ER+ ILC (Inclusion criteria: female, ≥ 10% ERα positivity, PR+/−, HER2 amplification negative, and had surgery for primary breast cancer at MedStar Georgetown University Hospital). Exclusion criteria were patients diagnosed with carcinoma *in situ* only, known *BRCA* or other familial mutation carriers, and evidence of neoadjuvant therapy. All patients were consented through the Histopathology and Tissue Shared Resource, (HTSR), the Survey, Recruitment, and Biospecimen Shared Resource (SRBSR), or IndivuMed under the following respective Georgetown University IRB protocols: 1992-048, Pr0000007, and 2007-345. Demographic, clinical, and pathological data, comorbidities, vital status, and follow-up time (vital status and follow-up time updated July 2021) are shown in **Table 1**.

OPAL Multiplex IHC and Image Processing. Duplicate sections of each TMA, taken from different depths, were subjected to multiplex IHC conducted on the Vectra3 multispectral imaging platform (Akoya Biosciences, Marlborough, MA) using OPAL chemistry as previously described[14] . Antibody/OPAL pairing and staining order was empirically determined by several criteria, including spectrally separating co-localized markers and separating spectrally adjacent dyes. We first performed singleplex IHC with the chosen antibody/OPAL dye pair to optimize signal intensity values and gauge proper cellular expression, followed by optimizing the entire multiplex assay. Primary antibodies in the panel, OPAL pairing, and other methodological details are shown in **Supplemental Table 1**. Image scanning, spectral unmixing, tissue/cell segmentation, phenotyping, and analysis on the Vectra 3.0 Automated Quantitative Pathology Imaging System using Phenochart and inForm 2.4.6 (PerkinElmer/Akoya) was conducted as previously described[14] . Data (percent cell positivity) from replicate cores and duplicate TMA sections for each tumor were averaged.

Statistical Analyses. GraphPad Prism 10 (Boston, MA, RRID:SCR_002798) was used for statistical analyses. Mann Whitney tests were used to analyze and compare protein expression in lobular vs. ductal tumor (panCK+) and stromal cells (panCK-), and by lymph node-positive vs. negative status. Simple linear regression and Spearman ρ correlation analyses were used to compare protein expression versus tumor size or patient age, and co-expression between proteins in tumor and stroma. Kaplan-Meier analyses and log-rank tests were used for overall survival analysis. Fisher's exact and Chi-squared tests were used to analyze demographic, clinical and pathological data where appropriate, and the relationship between comorbidity or race and high vs low (above vs. below the median) protein expression. All relevant tests were two-sided and statistical significance was defined as $p \leq 0.05$. Asterisks denote statistical significance as follows: *, $p \leq 0.05$; **, $p \leq 0.01$; ***, $p \leq 0.001$; ****, $p \leq 0.0001$.

Results

Study population and cohort comparisons. We constructed a series of TMAs of ER+ ILC (n=72) and IDC/NST (n=50) for staining with our custom multiplex IHC panel (**Figure 1B, Table 1**). Our cohort is unique in having 34% of patients self-report their race as non-white, including 25% identifying as Black or African American, with equal representation in the ILC and IDC/NST cohorts. This is particularly notable for ILC, for which there is a paucity of data from non-white patient populations. Patients with ILC were younger than those with IDC/NST at diagnosis (54 vs 59y, **p=0.003). Many prior retrospective analyses suggest ILC occurs primarily in women >60y, which may be related to issues with detection of ILC. Likely consistent with younger age and a numerical trend towards shorter duration of follow-up, a significantly greater proportion of ILC patients were alive at last contact (85%, vs 64% for IDC/NST, ***p=0.001). Other clinicopathological features including nodal status and treatment modality were similar across cohorts. While our inclusion criteria required that tumors be ER+ and HER2 amplification negative, we compared ER, progesterone receptor (PR), and HER2 expression (Ki67 data were not available) from the original pathology reports. HER2 expression and percent PR+ were similar in ILC and IDC/NST (data not shown), but percent ER+ was slightly lower in ILC (83.5% vs 91% for IDC/NST, *p=0.02), which is consistent with a prior study[42].

Expression of glutamate-handling proteins in ILC vs. IDC/NST. We used three well-characterized public datasets[26–29] to compare mRNA expression of the four target proteins in our multiplex IHC panel in ILC, IDC/NST, and (where reported) mixed mDLC (**Figure S1A**). *SLC7A11* and *SLC3A2* expression are both significantly greater in IDC/NST compared to ILC in multiple datasets. This may in part be due to the fact that these analyses do not stratify by hormone receptor status, and xCT is often overexpressed in triple negative breast cancer[43], which is more prevalent in IDC/NST. By contrast, *GPX4* expression is significantly greater in ILC vs. IDC/NST in the METABRIC dataset, while *GLUD1* expression is significantly greater in ILC vs. IDC/NST in both the METABRIC and SCAN-B datasets. Prior studies in models of mammary epithelial cells show GLUD1 expression is elevated under quiescent and slower growth conditions[44], which is generally consistent with ILC's more indolent nature.

We used two of the best-characterized ER+ ILC cell lines and their endocrine therapy-resistant derivatives[36,37] , to measure the expression of the four target proteins by immunoblotting (**Figure S1B**). Tamoxifen-resistant LCCTam cells show modest (<2-fold) upregulation of SLC7A11, GLUD1/2, and GPX4 compared to the parental SUM44 cells. However, three of the four long-term estrogen-deprived cell lines (LTED, mimicking aromatase inhibitor resistance) derived from parental MDA-MB-134VI (MM134) cells exhibit robust, 2- to 6-fold upregulation of GPX4 and GLUD1/2, potentially suggestive of a role for these enzymes in aggressive or more advanced ILC.

In our TMAs, we compared the abundance of each target protein expressed, as a percentage of positive cells, in ILC vs. IDC/NST within the tumor (pan-cytokeratin-positive, panCK+ cells) and stromal (panCK- cells) compartments (**Figures 1B, S2**). Consistent with public mRNA data, but despite all tumors being ER+, SLC7A11 and SLC3A2 protein expression in tumor cells is more abundant in IDC/NST (40-45%) compared to ILC (<25%). In our cohort, GLUD1/2 expression in tumor cells is also significantly greater in IDC/NST, though expression in both cohorts is $\geq$50%, while there is no significant difference for GPX4 (~50% positive cells in both cohorts). In stromal or non-epithelial cells, SLC3A2 expression is significantly more abundant in IDC/NST, while GPX4 expression is significantly more abundant in ILC. Together these data suggest that while all four glutamate-handling proteins are expressed in ILC across multiple datasets and sample types, the intracellular enzymes GLUD1/2 and GPX4 are generally more prevalent in ILC vs. IDC/NST.

All four glutamate-handling proteins are each associated with increased tumor size in ILC. We assessed the relationship between the abundance of each protein in the tumor and stromal compartment, and known breast cancer prognostic factors, including lymph node status, age, and tumor size at diagnosis, using linear regression and Spearman ρ. We find no statistically significant relationship between any of these glutamate handling proteins and either lymph node status or age as a continuous variable (data not shown). However, SLC7A11, SLC3A2, GLUD1/2, and GPX4 expression in tumor cells is each positively and significantly associated with increased tumor size in ILC, but not IDC/NST (**Figure 2A, B**). GLUD1/2 and GPX4 expression in the stroma is also significantly correlated with larger tumors in the ILC cohort. Since larger tumor size is linked to shorter overall survival (OS) in breast cancer (e.g.[45]), we tested whether high vs. low (above vs. below median) protein expression for each target is associated with OS in our ILC and IDC/NST cohorts, which have a median follow-up time of 8.4 and 10.4 years, respectively (**Figure 2C**). Only high tumor cell SLC3A2 expression is significantly associated with shorter OS in ILC, but not IDC/NST. Together these data implicate multiple members of this network of glutamate-handling proteins –notably SLC3A2, GLUD1/2, and GPX4 – as poor prognostic factors in ILC.

Co-expression of glutamate-handling proteins in ILC. Since SLC3A2, SLC7A11, GPX4, and GLUD1/2 are all functionally related (Figure 1A), we assessed whether they are co-expressed – e.g. do ILC with a high percentage of cells expressing one of the proteins also have a high percentage of cells expressing one or more of the others (**Figure 3A**). There is moderate to strong significant co-expression amongst all four proteins in ILC. For example, in ILC, tumor cell GPX4 abundance is significantly associated with expression of every other protein in both compartments. There is also a significant positive correlation between tumor or stromal GLUD1/2 and ER expression. By contrast, in IDC/NST, tumor cell GPX4 abundance is only significantly positively associated with itself and SLC7A11 in stromal cells, and there is no correlation of any protein with either ER or PR expression (**Figure 3B**). These data show that the known functional relationships between these glutamate-handling proteins translate to increased co-expression in ILC, where all members of this network are significantly associated with increased tumor size.

SLC3A2, GPX4, and GLUD1/2 are strongly associated with increased tumor size in Black women with ILC. Racial disparities in breast cancer outcomes are most widely discussed in the context of triple negative breast cancer. However, Parab et al.[46] recently published that non-Hispanic Black or African-American women are significantly more likely to have aggressive ER+ breast tumors (defined by a high-risk recurrence score on the Oncotype DX panel) when compared to non-Hispanic white women. Van Alsten et al.[47] show similar data for the PAM50-based risk of recurrence score, wherein young (<50 years of age) Black women with ER+ breast cancer are more likely to have intermediate to high scores as compared to young white women. Consistent with this, Rauscher et al.[48] report the risk of death from ER+/PR+ breast cancer is more than four times higher for Black women as compared to white women, even after adjustment for tumor stage, grade, and delays in initiation of treatment, while a meta-analysis by Torres et al. shows Black women have a 50% higher relative risk of death from ER+ breast cancer[49].

Unfortunately, these (and most other) studies of racial disparities in ER+ breast cancer do not report the presence or absence of lobular histology, a point that is complicated by our poor understanding of the true prevalence of ILC in Black women. Analysis of publications that provide such data[50–55] indicate the prevalence of ILC in Black women ranges from 5.5% to 16% of breast cancers – a rate that, in some of these studies, is significantly lower compared to non-Hispanic white women within the same cohort (**Supplemental Table 2**). However, it is unclear whether

these studies are indeed representative of ILC incidence in Black women. This is further confounded by variability in diagnostic criteria for ILC in all populations[56,57].

Nevertheless, with sixteen out of 72 (22%) and fifteen out of 50 (30%) women in our ILC and IDC/NST cohorts, respectively, self-reporting their race as Black or African American (none self-report Hispanic ethnicity), we assessed the relationship between the abundance of each protein in the tumor and stromal compartments with tumor size specifically in Black women (**Figure 4A, B**). Tumor and stromal cell GPX4, GLUD1/2, and SLC3A2 abundance are each positively and significantly associated with increased tumor size in ILC, but not IDC/NST. For all these proteins, the association with tumor size is markedly stronger in Black women with ILC than in the full ILC cohort.

Adding to our poor understanding of the biology of ILC in Black women is the lack of racial diversity in publicly available datasets. METABRIC and SCAN-B report zero Black women with ILC, and current TCGA data report only thirteen (6.5%). We specifically analyzed *GLUD1* mRNA expression in relation to tumor stage in Black women with ILC or with luminal IDC/NST in the TCGA (**Figure 4C**), since this enzyme has the strongest correlation with tumor size (Spearman ρ=0.61) and is uniquely associated with ER expression in our ILC cohort (Figure 3A). Despite the low sample number, there is a clear, stage-dependent increase in *GLUD1* expression in tumors from Black women with ILC (**Figure 4C**). By contrast, there is a significant decrease in *GLUD1* expression in Stage II vs Stage I luminal IDC/NST in Black women. Of note, the top 100 genes positively correlated with *GLUD1* expression in TCGA tumors from Black women with ILC and IDC/NST are enriched for glutamine and glutamate metabolism (KEGG, q=0.011 and 0.044, respectively). However, in tumors from Black women with ILC, the top 100 *GLUD1*-associated genes also show significant enrichment for the synthesis of arginine (KEGG, q=0.011), N-glycans (KEGG, q=0.046), and uridine diphosphate N-acetylglucosamine (UDP-GlcNAc, Metabolomics Workbench Metabolites, q=0.018). With all of the uniquely ILC-enriched pathways linked to breast cancer progression and metastatic potential (e.g.[58,59]), these potentially provocative findings implicate GLUD1/2 as a poor prognostic factor with particular importance for Black women with ILC.

SLC3A2 and GPX4 enrichment in women with ILC and IDC/NST and comorbidities. Multiple comorbid conditions like hypertension, obesity and metabolic syndrome are linked to poor outcomes in breast cancer, and there are racial disparities in the prevalence of these comorbidities[60–63]. Abstraction of electronic health records shows no difference in the presence or absence of comorbidities by ICD-9-CM diagnosis codes (details in **Supplemental Table 3**). However, a significantly greater proportion of ILC patients reported hypertension as a comorbidity, while significantly more IDC/NST patients reported obesity (**Figure 5A**). Next, we compared comorbidity presence or absence between Black and white women, and assessed if high expression (above median) of any of these glutamate-handling proteins correlates with comorbidity in ILC and IDC/NST. Significantly more Black women have comorbid conditions in both cohorts (**Figure 5B**). High SLC3A2 expression is enriched in women with ILC who have comorbidities, while high GPX4 expression is enriched in women with IDC/NST who have comorbidities (**Figure 5C**). There is no relationship between high GLUD1/2 or SLC7A11 expression and comorbidities in either cohort, suggesting that the relationship we observe between GLUD1/2 and tumor size in ILC is likely not confounded by comorbidities. SLC3A2's enrichment in the presence of comorbidities in ILC is consistent with its relationship to significantly shorter OS in this cohort. GPX4's enrichment in the presence of comorbidities is perhaps

surprising, given that we find no relationship between GPX4 and either tumor size or OS in IDC/NST. In a transgenic mouse model, high fat diet-induced adiposity is significantly enhanced by overexpression of GPX4[64], though the relationship between GPX4 and obesity in humans remains to be resolved.

Pharmacological inhibition of GLUD1 reduces ER protein levels, increases ROS, and reduces oxidative phosphorylation in endocrine therapy-resistant ILC cell lines. Breast cancer laboratory models suffer the same lack of racial and ancestral diversity as most clinical cohorts. Nevertheless, we leveraged ILC cell lines to follow up on our novel observations that GLUD1/2 expression: 1) is significantly associated with increased tumor size in ILC (Figures 2 and 4); 2) is significantly associated with ER expression in ILC (Figure 3); and 3) is markedly increased in endocrine therapy-resistant variants of ER+ ILC cell lines (Figure S1B). Given its dual roles in TCA cycle anaplerosis and ammonia recycling, GLUD1/2 is predominantly localized to the mitochondria. However, a sub-population of GLUD1 has been reported in the nucleus, where it is involved in chromatin regulation and gene transcription in a catalytic activity-dependent manner[65,66]. Supporting a potential role for nuclear GLUD1 specifically in ILC, Sottnik et al. profiled ER-associated proteins in ILC by performing ER RIME (rapid immunoprecipitation mass spectrometry of endogenous proteins)[35]. GLUD1 was among ER-associated proteins specific to ILC cell lines (**Figure 6A**) that were not identified in prior ER RIME from IDC/NST cells[67]. To examine the potential role of GLUD1 in regulating ER expression, we treated a panel of six ER+ ILC cell lines with the GLUD1 inhibitor R162 (**Figure 6B**). R162 treatment markedly reduces ER expression in all six ILC cell lines.

GLUD1 has pro-tumorigenic roles in multiple malignancies that are attenuated by R162 treatment, which reduces alpha-ketoglutarate levels and induces cell death by blocking mitochondrial oxidative phosphorylation (OXPHOS) and/or increasing reactive oxygen species (ROS)[17,68–71]. We tested R162's effect on ROS production and cellular metabolism in the SUM44/LCCTam ILC cell line pair, because our prior work shows the resistant variant LCCTam is significantly more sensitive to inhibition of glutamate metabolism by Riluzole[14], evidenced by a greater reduction in cell growth and pro-survival kinase activation concomitant with increased lipid peroxidation (indicative of ferroptosis). Here, R162 significantly increases ROS production in the tamoxifen-resistant LCCTam variant, while the parental endocrine therapy-responsive SUM44 cell line is resistant to ROS induction by R162 (**Figure 6C**) and the TBHP positive control (data not shown). To assess metabolic reprogramming in response to R162 treatment, we used FLIM coupled with phasor analysis to image protein-bound vs. free NADH, which correlates with OXPHOS and glycolytic metabolism, respectively[14,38,72] . Like the positive control OXPHOS inhibitor oligomycin, R162 causes a marked rightward shift (increase) in the fractional intensity of free NADH, consistent with reduced OXPHOS and increased glycolytic metabolism in LCCTam cells (**Figure 6D**). Together, these preclinical data show that pharmacological inhibition of GLUD1 reduces ER expression, increases ROS production, and reprograms metabolism in ILC cells.

Discussion

ILC has emerged as a breast cancer histologic subtype that is more reliant on amino acid and lipid metabolism than glucose metabolism. Our prior studies specifically highlight the importance of glutamate signaling in ILC[13,14]. Here, we provide evidence for a relationship between a focused network of four glutamate-handling proteins (SLC3A2, SLC7A11, GPX4, and GLUD1/2) and increased tumor size in primary ILC, but not primary IDC/NST. SLC3A2, GPX4, and GLUD1/2 expression in tumor and stroma show a markedly stronger relationship with increased tumor size in Black women with ILC. Finally, a small-molecule inhibitor of GLUD1 reduces ER protein levels, increases ROS, and reduces OXPHOS in endocrine therapy-resistant ILC cell lines.

All four glutamate metabolism and transport proteins measured here each have a significant positive relationship with larger tumor size, and with each other, in ILC. Because a high degree of co-expression leads to multicollinearity that confounds multiple linear regression models, we do not report the results of these analyses. High expression of SLC3A2 is also associated with shorter OS and higher risk of having one or more comorbidities in our ILC cohort. Upregulation of SLC3A2 is associated with poor prognosis in multiple cancers[21,73,74] , including certain highly proliferative, c-Myc-driven breast cancers[22]. Recent studies show SLC3A2 is required for the growth of tamoxifen-resistant ER+ breast cancer cells[75]. Importantly, SLC3A2 is an obligate heterodimeric partner for multiple L-type transporters beyond SLC7A11, positioning this protein as a crucial node in a broader amino acid transport network.

GPX4 plays a key role in detoxifying lipid peroxides that accumulate in cells, thereby preventing ferroptosis[76,77]. Recent work by Hu et al. shows that endocrine therapy can sensitize ER+ IDC/NST cell lines to ferroptosis induction by GPX4 inhibitors[78], while in tamoxifen-resistant IDC/NST cell lines, activation of the RelB arm of the NF-kB pathway inhibits ferroptosis by upregulating GPX4[79] . It is not known whether RelB is a transcriptional regulator of GPX4 in ILC, but we see an increase in GPX4 expression in tamoxifen-resistant and LTED ILC cells (Figure S1B). Of note, GPX4 sits at the intersection of multiple pathways that confer heightened sensitivity to ferroptosis. Cell-cell interactions mediated by E-cadherin suppress ferroptosis due to activation of the Hippo pathway, and loss or inhibition of E-cadherin leads to increased vulnerability to ferroptosis[76,80] . Cell density also influences ferroptosis sensitivity in the presence of wild type E-cadherin. Cells cultured at low density with few cell-cell contacts more susceptible to cell death caused by ferroptosis via GPX4 inhibition than those cultured at high density[77]. In the stroma, ferroptosis and GPX4 are regulated by metabolic pathways that influence tumor crosstalk with the potential to alter cancer progression and response to treatment (discussed in[81,82]). With E-cadherin loss via *CDH1* mutation and a discohesive growth pattern with few cell-cell contacts both defining features of ILC that contribute to ferroptosis sensitivity, our data implicate GPX4 as an attractive target for therapeutic intervention in ILC that requires further exploration.

GLUD1/2 expression in the tumor and stromal compartments is strongly correlated with increased tumor size in Black women with ILC in our cohort, while *GLUD1* mRNA increases with tumor stage in ILC from Black women in TCGA (Figure 4). By contrast, there is an inverse or negative relationship between GLUD1/2 and tumor size, and *GLUD1* and tumor stage in luminal IDC/NST, in our cohort and in TCGA data, respectively. Our observations contradict the findings of Craze et al.[83], who showed that *GLUD1* mRNA decreases with tumor grade, while both mRNA and protein are associated with better breast cancer-specific survival. Although their study included ILC cases (~8%), the analyses did not separate or compare ILC with IDC. Also in that work, the IDC/NST category explicitly included mDLC, which we now appreciate as highly heterogeneous

and perhaps a distinct entity[84]. Additional findings from our preclinical studies further support our conclusion that GLUD1/2 expression may confer poor prognosis in ILC. GLUD1/2 is increased in tamoxifen-resistant and LTED ILC cells, has a novel physical interaction with ER in ILC cell lines, and pharmacological inhibition of GLUD1 markedly reduces ER protein expression in multiple ILC cell lines (Figures S1B and 6, respectively). Placed in the context of current literature demonstrating ER's novel transcriptional regulatory functions and coregulators in ILC[35,37,85], and the role of a nuclear GLUD1 sub-population in chromatin remodeling and gene transcription[65,66], we propose that GLUD1/2:ER interactions may confer ILC-specific ER activities that could be targeted by GLUD1/2 inhibition, alone or in combination with endocrine therapies. It is important to point out that while we show pharmacological inhibition of GLUD1/2 in tamoxifen-resistant LCCTam cells leads to induction of ROS and a concomitant decrease in OXPHOS, further studies are needed to distinguish the well-studied mitochondrial functions of GLUD1/2 from its still-emerging roles in the nucleus.

There are several limitations to consider in the interpretation of this study. This is a single-institution, relatively small cohort, despite better proportional representation of Black or African American women than other published studies of ILC. Self-reported race is an important social construct, but ancestry informative marker-guided analyses will be integral to follow-up studies, as will access to more comprehensive data on comorbidities and systemic and social determinants of health that are potential mediators of breast cancer disparities. This latter point is particularly relevant because several of the proteins studied here have mechanistic connections to biological readouts for stress (such as allostatic load) that is disproportionately experienced by minoritized or marginalized communities, and/or associated with higher breast cancer risk or poorer outcomes[86–89]. Very limited studies have yet specifically examined systemic and social determinants of health in ILC (e.g.[90]).

Despite these limitations, our findings implicate this focused network of glutamate transport proteins and metabolic enzymes as a potentially important regulator of tumor growth and therapeutic response in ILC, with several network members being tractable targets for therapeutic intervention.

Author Contributions:
Conception and design: TAY, SB, RBR
Provision of study materials: AMR, KC, BTH
Collection and assembly of data: TAY, SB, TCA, EAP, ATR, NH, SP, AIF, DM, AOO, SR, JLS, MJS
Data analysis and interpretation: TAY, SB, TCA, EAP, ATR, AOO, SR, JLS, MJS, ZME
Manuscript writing: All authors.
Final approval of manuscript: All authors.
Accountable for all aspects of the work: All authors.

Ethical Approvals: All patients whose breast tumor samples were included on the TMAs were research-consented through the Histopathology and Tissue Shared Resource, (HTSR), the Survey, Recruitment, and Biospecimen Shared Resource (SRBSR), and/or IndivuMed under the following respective Georgetown University IRB protocols: 1992-048, Pr0000007, and 2007-345.

Preprints, Prior Publication, and Author Self-Archiving: The Author's Original Version of this manuscript has been preprinted at bioRxiv. This does not infringe any subsequent copyright or license agreement.

Acknowledgements: We wish to thank members of the Riggins Lab, NR IMPACT, Hackensack Meridian Health-John Theurer Cancer Center Community Advisory Council, Drs. Anju Duttargi and Raneen Rahhal, and Mr. Roberto D'Angelo-Cosme for their insights and helpful suggestions. Figures 1A and 1B were created with BioRender (https://biorender.com). This work was financially supported by Department of Defense Breast Cancer Research Program Award W81XWH-17-1-0615 to RBR, by CCSG Developmental Funds to SR from NIH/NCI Cancer Center Support Grant P30 CA051008 (principal investigator Dr. Louis Weiner), and by NIH/NCI R00 CA193734 and R01CA251621 to MJS. Fellowship funding for TAY was provided by the Tumor Biology Training Grant T32 CA009686 (principal investigator Dr. Anna Riegel). TAY also received a travel award to present a portion of this work at the 2023 Endocrine Society Annual Meeting. Fellowship funding for TCA and EAP was provided by American Cancer Society (ACS) Diversity in Cancer Research awards IRG-17-177-23-IRG and DICR INTR-23-1253711-01-DICR INTR (principal investigator RBR). TCA also received a travel award to present a portion of this work at the 2023 Annual Biomedical Research Conference for Minoritized Scientists (ABRCMS). SP received a Georgetown Undergraduate Research Opportunities Program (GUROP) Summer Fellowship. DM received a Summer Mentored Undergraduate Research Fellowship (SMURF) award from Georgetown University, and support from a 2024-2025 Goldwater Scholar award. Technical services were provided by the TCBSR, HTSR, SRBSR, MISR, and FCSR, as described in the Methods section, which are supported in part by NIH/NCI Cancer Center Support Grant P30 CA051008 (principal investigator Dr. Louis Weiner). The content of this article is the sole responsibility of the authors and does not represent the official view of the DoD, NIH, or ACS.

Abbreviations

[^{18}F]FDG-PET, 18F-fluorodeoxyglucose positron emission tomography; Asp, aspartic acid; Cys, cyst(e)ine; DIVER, Deep Imaging Via Emission Recovery; ER+, Estrogen Receptor Positive; FLIM, Fluorescent Lifetime Imaging; GEXPLORER, Gene Expression eXPLORER; Gln, glutamine; Glu, glutamate; GLUD1/2 or GDH1/2, Glutamate Dehydrogenase 1/2; Gly, glycine; GPX4, Glutathione Peroxidase 4; GSH, glutathione; GSSG, glutathione disulfide; IDC/NST, Invasive Ductal, or Breast Cancer of No Special Type; IHC, Immunohistochemistry; ILC, Invasive

Lobular Breast Cancer; LCCTam, Tamoxifen-resistant Derivative of SUM44PE; Leu, leucine; LTED, Long-term Estrogen-deprived Derivative of MDA-MB-134VI; mDLC, Mixed Ductal-lobular Breast Cancer; mGluRs, Metabotropic Glutamate Receptors; OXPHOS, Oxidative Phosphorylation; RIME, Rapid Immunoprecipitation Mass Spectrometry of Endogenous Proteins; panCK, Pan-cytokeratin; Pro, proline; R162, GLUD1 inhibitor; ROS, Reactive Oxygen Species; SCAN-B, Sweden Cancerome Analysis Network – Breast; TBHP, Tert-Butyl Hydroperoxide; TCA, tricarboxylic acid; TCGA, The Cancer Genome Atlas; TMA, Tissue Microarray.

References

1. Christgen, M. *et al.* Lobular Breast Cancer: Histomorphology and Different Concepts of a Special Spectrum of Tumors. *Cancers* **13**, 3695 (2021).
2. McCart Reed, A. E., Kalinowski, L., Simpson, P. T. & Lakhani, S. R. Invasive lobular carcinoma of the breast: the increasing importance of this special subtype. *Breast Cancer Res* **23**, 6 (2021).
3. Ciriello, G. *et al.* Comprehensive Molecular Portraits of Invasive Lobular Breast Cancer. *Cell* **163**, 506–19 (2015).
4. Ulaner, G. A. & Schuster, D. M. Amino Acid Metabolism as a Target for Breast Cancer Imaging. *PET Clin* **13**, 437–444 (2018).
5. Savir-Baruch, B., Zanoni, L. & Schuster, D. M. Imaging of Prostate Cancer Using Fluciclovine. *PET Clin* **12**, 145–157 (2017).
6. Ulaner, G. A. *et al.* Initial Results of a Prospective Clinical Trial of 18F-Fluciclovine PET/CT in Newly Diagnosed Invasive Ductal and Invasive Lobular Breast Cancers. *J. Nucl. Med.* **57**, 1350–1356 (2016).
7. Ulaner, G. A. *et al.* Prospective Clinical Trial of 18F-Fluciclovine PET/CT for Determining the Response to Neoadjuvant Therapy in Invasive Ductal and Invasive Lobular Breast Cancers. *J. Nucl. Med.* **58**, 1037–1042 (2017).
8. Mushtaq, A. *et al.* Prospective investigation of amino acid transport and PSMA-targeted positron emission tomography for metastatic lobular breast carcinoma. *Eur J Nucl Med Mol Imaging* (2024) doi:10.1007/s00259-024-06830-7.
9. Du, T. *et al.* Key regulators of lipid metabolism drive endocrine resistance in invasive lobular breast cancer. *Breast Cancer Res.* **20**, 106 (2018).
10. Du, T. *et al.* Invasive lobular and ductal breast carcinoma differ in immune response, protein translation efficiency and metabolism. *Sci Rep* **8**, 7205 (2018).

11. Cha, Y. J., Kim, H. M. & Koo, J. S. Expression of Lipid Metabolism-Related Proteins Differs between Invasive Lobular Carcinoma and Invasive Ductal Carcinoma. *Int JMol Sci* **18**, 232 (2017).
12. Sottnik, J. L. *et al.* WNT4 Regulates Cellular Metabolism via Intracellular Activity at the Mitochondria in Breast and Gynecologic Cancers. *Cancer Res Commun* **4**, 134–151 (2024).
13. Stires, H. *et al.* Integrated molecular analysis of Tamoxifen-resistant invasive lobular breast cancer cells identifies MAPK and GRM/mGluR signaling as therapeutic vulnerabilities. *Mol Cell Endocrinol* **471**, 105–117 (2018).
14. Olukoya, A. O. *et al.* Riluzole Suppresses Growth and Enhances Response to Endocrine Therapy in ER+ Breast Cancer. *J Endocr Soc* **7**, bvad117 (2023).
15. Bahnassy, S., Sikora, M. J. & Riggins, R. B. Unlocking the Mysteries of Lobular Breast Cancer Biology Needs the Right Combination of Preclinical Models. *Mol Cancer Res* **20**, 837–840 (2022).
16. Sikora, M. J. & Ostrander, J. H. A Path to Precision Metabolic Treatment in Breast Cancer: Riluzole, Glutamate Signaling, and Invasive Lobular Carcinoma. *J Endocr Soc* **8**, bvad171 (2024).
17. Ma, Z. *et al.* Glutamate dehydrogenase 1: A novel metabolic target in inhibiting acute myeloid leukaemia progression. *Br J Haematol* **202**, 566–577 (2023).
18. Spinelli, J. B. *et al.* Metabolic recycling of ammonia via glutamate dehydrogenase supports breast cancer biomass. *Science* **358**, 941–946 (2017).
19. Liu, J., Xia, X. & Huang, P. xCT: A Critical Molecule That Links Cancer Metabolism to Redox Signaling. *Mol Ther* **28**, 2358–2366 (2020).
20. Shin, S.-S. *et al.* Participation of xCT in melanoma cell proliferation in vitro and tumorigenesis in vivo. *Oncogenesis* **7**, 86 (2018).
21. Xia, P. & Dubrovska, A. CD98 heavy chain as a prognostic biomarker and target for cancer treatment. *Front. Oncol.* **13**, (2023).

22. El Ansari, R. *et al.* The multifunctional solute carrier 3A2 (SLC3A2) confers a poor prognosis in the highly proliferative breast cancer subtypes. *Br J Cancer* **118**, 1115–1122 (2018).
23. Ye, L. *et al.* Metabolism-regulated ferroptosis in cancer progression and therapy. *Cell Death Dis* **15**, 1–12 (2024).
24. Okazaki, S. *et al.* Glutaminolysis-related genes determine sensitivity to xCT-targeted therapy in head and neck squamous cell carcinoma. *Cancer Sci* **110**, 3453–3463 (2019).
25. Zhang, X. *et al.* Endogenous glutamate determines ferroptosis sensitivity via ADCY10-dependent YAP suppression in lung adenocarcinoma. *Theranostics* **11**, 5650–5674 (2021).
26. Liu, J. *et al.* An Integrated TCGA Pan-Cancer Clinical Data Resource to Drive High-Quality Survival Outcome Analytics. *Cell* **173**, 400-416.e11 (2018).
27. Pereira, B. *et al.* The somatic mutation profiles of 2,433 breast cancers refines their genomic and transcriptomic landscapes. *Nat Commun* **7**, 11479 (2016).
28. Saal, L. H. *et al.* The Sweden Cancerome Analysis Network - Breast (SCAN-B) Initiative: a large-scale multicenter infrastructure towards implementation of breast cancer genomic analyses in the clinical routine. *Genome Med* **7**, 20 (2015).
29. Brueffer, C. *et al.* The mutational landscape of the SCAN-B real-world primary breast cancer transcriptome. *EMBO Mol Med* **12**, e12118 (2020).
30. Cerami, E. *et al.* The cBio cancer genomics portal: an open platform for exploring multidimensional cancer genomics data. *Cancer Discov* **2**, 401–4 (2012).
31. Gao, J. *et al.* Integrative analysis of complex cancer genomics and clinical profiles using the cBioPortal. *Sci Signal* **6**, pl1 (2013).
32. Xie, Z. *et al.* Gene Set Knowledge Discovery with Enrichr. *Current Protocols* **1**, e90 (2021).
33. Kuleshov, M. V. *et al.* Enrichr: a comprehensive gene set enrichment analysis web server 2016 update. *Nucleic Acids Res* **44**, W90-97 (2016).
34. Chen, E. Y. *et al.* Enrichr: interactive and collaborative HTML5 gene list enrichment analysis tool. *BMC Bioinformatics* **14**, 128 (2013).

35. Sottnik, J. L. *et al.* Mediator of DNA Damage Checkpoint 1 (MDC1) Is a Novel Estrogen Receptor Coregulator in Invasive Lobular Carcinoma of the Breast. *Mol Cancer Res* **19**, 1270–1282 (2021).
36. Riggins, R. B. *et al.* ERRgamma Mediates Tamoxifen Resistance in Novel Models of Invasive Lobular Breast Cancer. *Cancer Res.* **68**, 8908–8917 (2008).
37. Sikora, M. J. *et al.* WNT4 mediates estrogen receptor signaling and endocrine resistance in invasive lobular carcinoma cell lines. *Breast Cancer Res* **18**, 92 (2016).
38. Ranjit, S., Malacrida, L., Jameson, D. M. & Gratton, E. Fit-free analysis of fluorescence lifetime imaging data using the phasor approach. *Nat Protoc* **13**, 1979–2004 (2018).
39. Malacrida, L., Ranjit, S., Jameson, D. M. & Gratton, E. The Phasor Plot: A Universal Circle to Advance Fluorescence Lifetime Analysis and Interpretation. *Annu Rev Biophys* **50**, 575–593 (2021).
40. Stringari, C. *et al.* Metabolic trajectory of cellular differentiation in small intestine by Phasor Fluorescence Lifetime Microscopy of NADH. *Sci Rep* **2**, 568 (2012).
41. Fernandez, A. I. *et al.* The orphan nuclear receptor estrogen-related receptor beta (ERRβ) in triple-negative breast cancer. *Breast Cancer Res Treat* **179**, 585–604 (2020).
42. Sreekumar, S. *et al.* Differential regulation and targeting of estrogen receptor α turnover in invasive lobular breast carcinoma. *Endocrinology* (2020) doi:10.1210/endocr/bqaa109.
43. Timmerman, L. A. *et al.* Glutamine sensitivity analysis identifies the xCT antiporter as a common triple-negative breast tumor therapeutic target. *Cancer Cell* **24**, 450–465 (2013).
44. Coloff, J. L. *et al.* Differential Glutamate Metabolism in Proliferating and Quiescent Mammary Epithelial Cells. *Cell Metab* **23**, 867–880 (2016).
45. Michaelson, J. S. *et al.* Predicting the survival of patients with breast carcinoma using tumor size. *Cancer* **95**, 713–723 (2002).
46. Parab, A. Z. *et al.* Socioecologic Factors and Racial Differences in Breast Cancer Multigene Prognostic Scores in US Women. *JAMA Network Open* **7**, e244862 (2024).

47. Van Alsten, S. C. *et al.* Differences in 21-Gene and PAM50 Recurrence Scores in Younger and Black Women With Breast Cancer. *JCO Precis Oncol* e2400137 (2024) doi:10.1200/PO.24.00137.

48. Rauscher, G. H. *et al.* Racial disparity in survival from estrogen and progesterone receptor positive breast cancer: implications for reducing breast cancer mortality disparities. *Breast Cancer Res Treat* **163**, 321 (2017).

49. Torres, J. M., Sodipo, M. O., Hopkins, M. F., Chandler, P. D. & Warner, E. T. Racial Differences in Breast Cancer Survival Between Black and White Women According to Tumor Subtype: A Systematic Review and Meta-Analysis. *J Clin Oncol* JCO2302311 (2024) doi:10.1200/JCO.23.02311.

50. Baquet, C. R., Mishra, S. I., Commiskey, P., Ellison, G. L. & DeShields, M. Breast cancer epidemiology in blacks and whites: disparities in incidence, mortality, survival rates and histology. *J Natl Med Assoc* **100**, 480–488 (2008).

51. Elledge, R. M., Clark, G. M., Chamness, G. C. & Osborne, C. K. Tumor Biologic Factors and Breast Cancer Prognosis Among White, Hispanic, and Black Women in the United States 1. *J Natl Cancer Inst* **86**, 705–712 (1994).

52. Gallagher, E. J. *et al.* Insulin resistance and racial disparities in breast cancer prognosis: a multi-center cohort study. *Endocr Rel Cancer* (2022) doi:10.1530/ERC-22-0106.

53. Han, Y. *et al.* Breast Cancer Mortality Hot Spots Among Black Women With de Novo Metastatic Breast Cancer. *JNCI Cancer Spectr* **5**, pkaa086 (2021).

54. Oesterreich, S. *et al.* Clinicopathological Features and Outcomes Comparing Patients With Invasive Ductal and Lobular Breast Cancer. *J Natl Cancer Inst* **114**, 1511–1522 (2022).

55. Williams, L. A. *et al.* Reproductive risk factor associations with lobular and ductal carcinoma in the Carolina Breast Cancer Study. *Cancer Causes Control* **29**, 25–32 (2018).

56. De Schepper, M. *et al.* Integration of Pathological Criteria and Immunohistochemical Evaluation for Invasive Lobular Carcinoma Diagnosis: Recommendations From the European Lobular Breast Cancer Consortium. *Mod Pathol* **37**, 100497 (2024).
57. Djerroudi, L. *et al.* E-Cadherin Mutational Landscape and Outcomes in Breast Invasive Lobular Carcinoma. *Mod Pathol* **37**, 100570 (2024).
58. Oikari, S. *et al.* UDP-sugar accumulation drives hyaluronan synthesis in breast cancer. *Matrix Biol* **67**, 63–74 (2018).
59. Niu, F. *et al.* Arginase: An emerging and promising therapeutic target for cancer treatment. *Biomedicine & Pharmacotherapy* **149**, 112840 (2022).
60. Nyrop, K. A. *et al.* Obesity, comorbidities, and treatment selection in Black and White women with early breast cancer. *Cancer* **127**, 922–930 (2021).
61. Han, H. *et al.* Hypertension and breast cancer risk: a systematic review and meta-analysis. *Sci Rep* **7**, 44877 (2017).
62. Anwar, S. L. *et al.* Metabolic comorbidities and the association with risks of recurrent metastatic disease in breast cancer survivors. *BMC Cancer* **21**, 590 (2021).
63. Monzavi-Karbassi, B. *et al.* Pre-diagnosis blood glucose and prognosis in women with breast cancer. *Cancer & Metab* **4**, 7 (2016).
64. Hall, S. *et al.* GPX4 Over-expression Is Associated with Increased Senescence Burden and Metabolic Dysfunction. *Physiology* **39**, 1782 (2024).
65. Su, X. B. & Pillus, L. Functions for diverse metabolic activities in heterochromatin. *Proc Natl Acad Sci USA* **113**, E1526–E1535 (2016).
66. Traube, F. R. *et al.* Redirected nuclear glutamate dehydrogenase supplies Tet3 with α-ketoglutarate in neurons. *Nat Commun* **12**, 4100 (2021).
67. Mohammed, H. *et al.* Endogenous purification reveals GREB1 as a key estrogen receptor regulatory factor. *Cell Rep* **3**, 342–349 (2013).

68. Mi, W. *et al.* BET inhibition induces GDH1-dependent glutamine metabolic remodeling and vulnerability in liver cancer. *Life Metabolism* **3**, loae016 (2024).
69. Kang, J. *et al.* EGFR-phosphorylated GDH1 harmonizes with RSK2 to drive CREB activation and tumor metastasis in EGFR-activated lung cancer. *Cell Rep* **41**, 111827 (2022).
70. Jin, L. *et al.* Glutamate dehydrogenase 1 signals through antioxidant glutathione peroxidase 1 to regulate redox homeostasis and tumor growth. *Cancer Cell* **27**, 257–270 (2015).
71. Wang, Q. *et al.* Therapeutic targeting of glutamate dehydrogenase 1 that links metabolic reprogramming and Snail-mediated epithelial-mesenchymal transition in drug-resistant lung cancer. *Pharmacol Res* **185**, 106490 (2022).
72. Ranjit, S., Datta, R., Dvornikov, A. & Gratton, E. Multicomponent Analysis of Phasor Plot in a Single Pixel to Calculate Changes of Metabolic Trajectory in Biological Systems. *J Phys Chem A* **123**, 9865–9873 (2019).
73. Bajaj, J. *et al.* CD98-Mediated Adhesive Signaling Enables the Establishment and Propagation of Acute Myelogenous Leukemia. *Cancer Cell* **30**, 792–805 (2016).
74. Kawasaki, Y., Omori, Y., Suzuki, S. & Yamada, T. CD98hc as a marker of radiotherapy-resistant cancer stem cells in head and neck squamous cell carcinoma. *Arch Med Sci* **19**, 1859–1868 (2023).
75. Saito, Y. *et al.* Polarity protein SCRIB interacts with SLC3A2 to regulate proliferation and tamoxifen resistance in ER+ breast cancer. *Commun Biol* **5**, 1–10 (2022).
76. Wu, J. *et al.* Intercellular interaction dictates cancer cell ferroptosis via NF2-YAP signalling. *Nature* **572**, 402–406 (2019).
77. Panzilius, E. *et al.* Cell density-dependent ferroptosis in breast cancer is induced by accumulation of polyunsaturated fatty acid-enriched triacylglycerides. *bioRxiv* 417949 (2019) doi:10.1101/417949.

78. Hu, K. *et al.* Efficacy of FERscore in predicting sensitivity to ferroptosis inducers in breast cancer. *NPJ Breast Cancer* **10**, 74 (2024).
79. Xu, Z. *et al.* RelB-activated GPX4 inhibits ferroptosis and confers tamoxifen resistance in breast cancer. *Redox Biol* **68**, 102952 (2023).
80. Minikes, A. M. *et al.* E-cadherin is a biomarker for ferroptosis sensitivity in diffuse gastric cancer. *Oncogene* **42**, 848–857 (2023).
81. Mbah, N. E. & Lyssiotis, C. A. Metabolic regulation of ferroptosis in the tumor microenvironment. *J Biol Chem* **298**, 101617 (2022).
82. Liu, Y., Duan, C., Dai, R. & Zeng, Y. Ferroptosis-mediated Crosstalk in the Tumor Microenvironment Implicated in Cancer Progression and Therapy. *Front. Cell Dev. Biol.* **9**, 739392 (2021).
83. Craze, M. L. *et al.* Glutamate dehydrogenase (GLUD1) expression in breast cancer. *Breast Cancer Res Treat* **174**, 79–91 (2019).
84. Shah, O. S. *et al.* Spatial molecular profiling of mixed invasive ductal and lobular breast cancers reveals heterogeneity in intrinsic molecular subtypes, oncogenic signatures, and mutations. *Proc Natl Acad Sci USA* **121**, e2322068121 (2024).
85. Shackleford, M. T. *et al.* Estrogen Regulation of mTOR Signaling and Mitochondrial Function in Invasive Lobular Carcinoma Cell Lines Requires WNT4. *Cancers* **12**, 2931 (2020).
86. Santaliz-Casiano, A. *et al.* Identification of metabolic pathways contributing to ER+ breast cancer disparities using a machine-learning pipeline. *Sci Rep* **13**, 12136 (2023).
87. Bobba-Alves, N. *et al.* Cellular allostatic load is linked to increased energy expenditure and accelerated biological aging. *Psychoneuroendocrinology* **155**, 106322 (2023).
88. Lee, M. *et al.* Assessing the Correlation between Allostatic Load and False-Positive Image-Guided Breast Biopsies. *J Womens Health (Larchmt)* (2024) doi:10.1089/jwh.2024.0039.

89. Wang, F. *et al.* Allostatic load and risk of invasive breast cancer among postmenopausal women in the U.S. *Prev Med* **178**, 107817 (2024).

90. Kaur, M. *et al.* Area Deprivation Index in Patients with Invasive Lobular Carcinoma of the Breast: Associations with Tumor Characteristics and Outcomes. *Cancer Epidemiol Biomarkers Prev* **32**, 1107–1113 (2023).

Table 1. Clinical and pathological characteristics of TMA cohorts

	ILC		IDC/NST		P value
	Count	Percent	Count	Percent	
Cohort period	2003-2014	-	2004-2011	-	
Number of patients	72	-	50	-	
Number of surgical events	78	-	50	-	
Sex					
Female	72	100%	50	100%	
Age					
Under 40	0	0%	3	6%	
40-55	37	51%	17	34%	
Over 55	35	49%	30	60%	
Age, initial diagnosis (years)	40.23 - 88.05	-	30.7-90.14	-	
Median age, initial diagnosis (years)	54.05	-	59	-	**p = 0.003
Race					
Black	16	22%	15	30%	p = 0.436
Other+Unknown	6	8%	4	8%	
White	50	70%	31	62%	
Lymph Node Status					
Positive	23	32%	18	36%	p = 0.655
Negative	49	68%	32	64%	
Vital Status (as of 7/2021)					
Alive	61	85%	32	64%	***p = 0.001
Deceased	11	15%	18	36%	
Duration of Follow-up (as of 7/2021)					
Range (years)	1.49 - 17.23	-	1.06-17.24	-	
Median (years)	8.42	-	10.36	-	p = 0.070
Treatment Received					
Chemotherapy	33	46%	29	59%	p = 0.202
Radiotherapy	34	47%	21	42%	p = 0.585
Endocrine Therapy	51	71%	35	71%	p > 0.999
Immunotherapy	1	1%	2	4%	p = 0.567

Figure 1. Expression of glutamate-handling proteins in ILC and IDC/NST. A, Schematic showing functional relationships between the four glutamate-handling proteins included in our multiplex IHC panel. Gln, glutamine; Glu, glutamate; Cys, cyst(e)ine; Gly, glycine; Pro, proline; Asp, aspartic acid; Leu, leucine; GSH, glutathione. **B**, Schema of cohort assembly and study workflow. A representative TMA core stained for the four target proteins and DNA is shown, along with its corresponding images processed for tissue segmentation indicating areas of panCK+ (yellow, epithelial) and panCK- (aqua, stromal) cells, followed by phenotype mapping for (as an example) GLUD1/2+ (magenta) and GLUD1/2- (blue) cells. **C**, Comparison of protein expression for GPX4 and GLUD1/2 in the multiplex IHC panel between ILC and IDC/NST in panCK+ tumor cells (left) and panCK- stromal cells (right). Data are presented as a scatter plot, with each dot the mean of percent positive cells for an individual patient tumor and the solid line indicating the median. Data are analyzed by Mann-Whitney U test.

Figure 1

A.

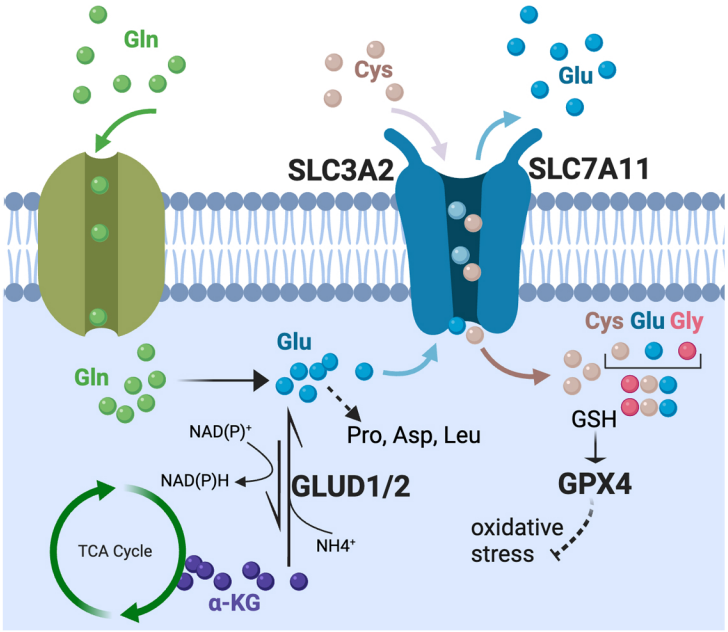

B.

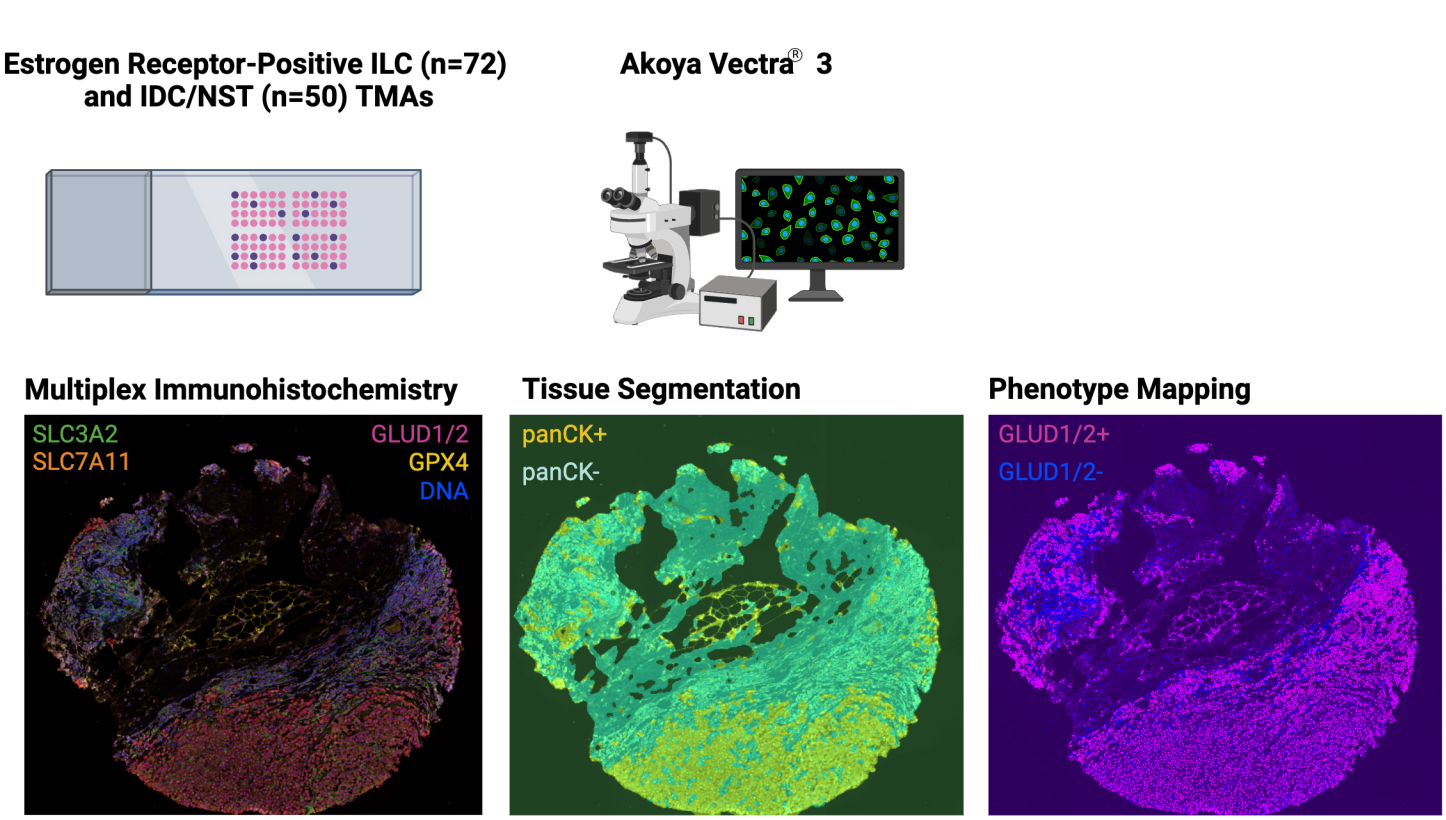

C.

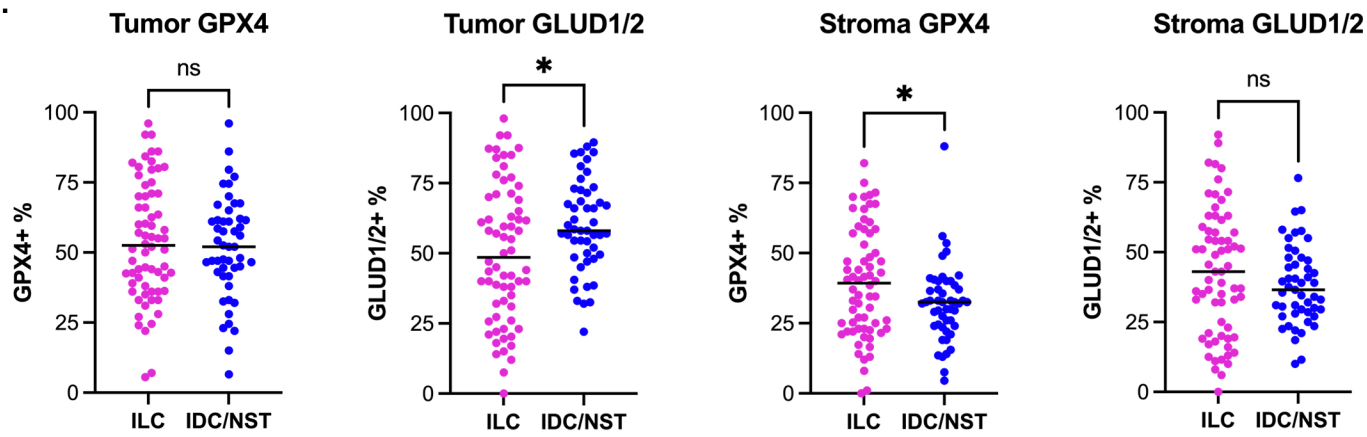

Figure 2. Glutamate-handling proteins are associated with increased tumor size in ILC. A, Graphs illustrating the relationship between tumor size (cm) and percent positive cells for tumor expression of GPX4 and GLUD1/2 in the ILC cohort. **B**, Spearman correlation coefficient (ρ) and p value for each protein's relationship to tumor size in panCK+ tumor cells and panCK- stromal cells for the ILC and IDC/NST cohorts. **C**, Kaplan-Meier survival analysis, log-rank p value, hazard ratio (HR), and 95% confidence interval (CI) for high (above median) versus low (below median) tumor expression (percent positive cells) of SLC3A2 in the ILC and IDC/NST cohorts.

Figure 2

A.

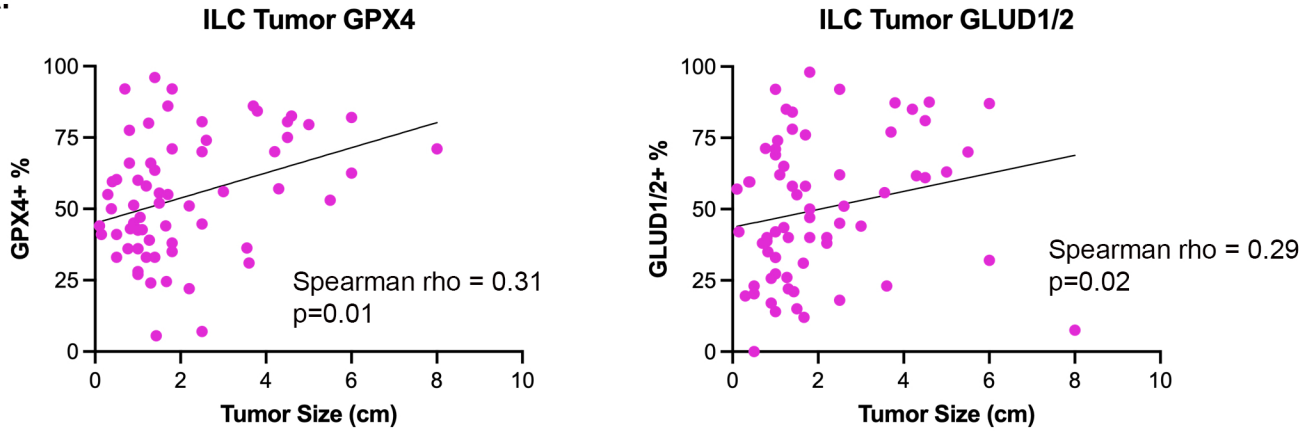

B.

Expression vs Tumor Size				
Tumor				
Protein	**ILC Spearman ρ**	**ILC P Value**	**IDC/NST Spearman ρ**	**IDC/NST P Value**
GPX4	0.3153	0.0099**	0.02268	0.8784
GLUD1/2	0.2933	0.0168*	0.007924	0.9574
SLC3A2	0.2951	0.0162*	-0.03899	0.7925
SLC7A11	0.2719	0.0272*	-0.02526	0.8647
Stroma				
Protein	**ILC Spearman ρ**	**ILC P Value**	**IDC/NST Spearman ρ**	**IDC/NST P Value**
GPX4	0.2457	0.0467*	0.09263	0.5312
GLUD1/2	0.2484	0.0443*	-0.04844	0.7437
SLC3A2	0.03266	0.7946	-0.2197	0.1334
SLC7A11	0.2152	0.0827	-0.1506	0.3069

C.

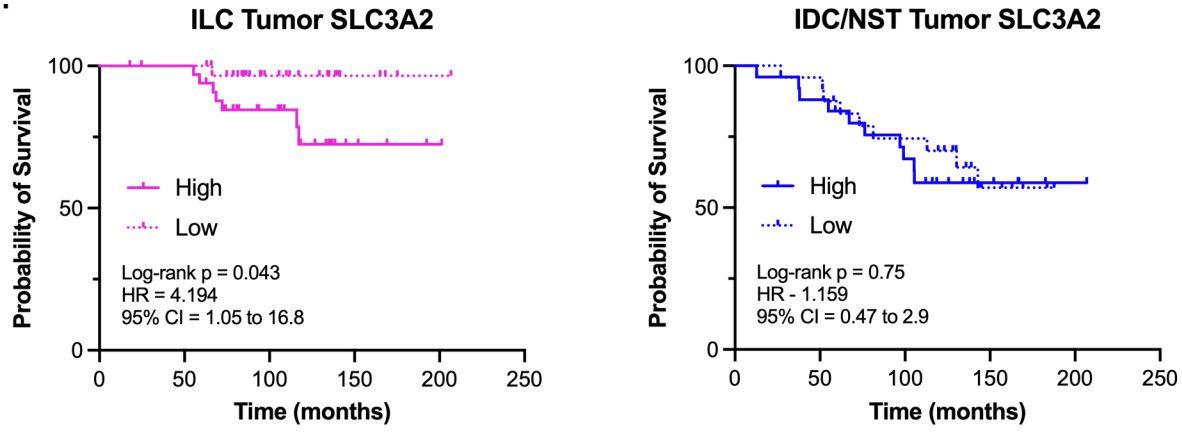

Figure 3. Increased co-expression of glutamate transport proteins and metabolic enzymes in ILC. Heatmaps showing Spearman correlation coefficients (ρ, ranging from +1.0 to -1.0) for each protein's relationship to another, and hormone receptor expression (percent positive cells), in the ILC (**A**) and IDC/NST (**B**) cohorts. Asterisks denote statistical significance as defined in the Methods section.

Figure 3

A. ILC

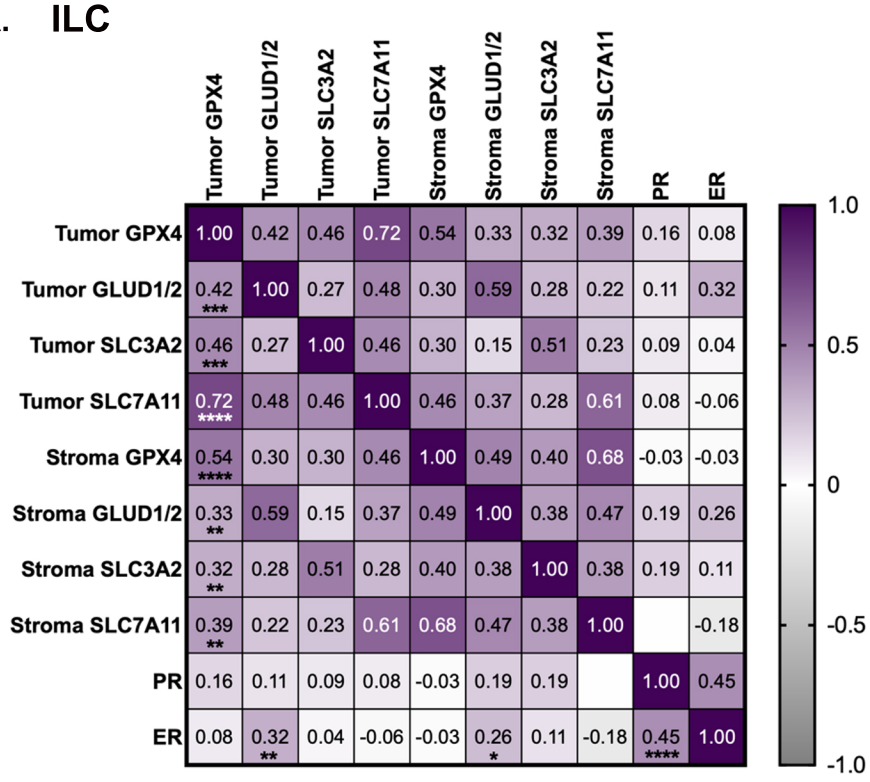

B. IDC/NST

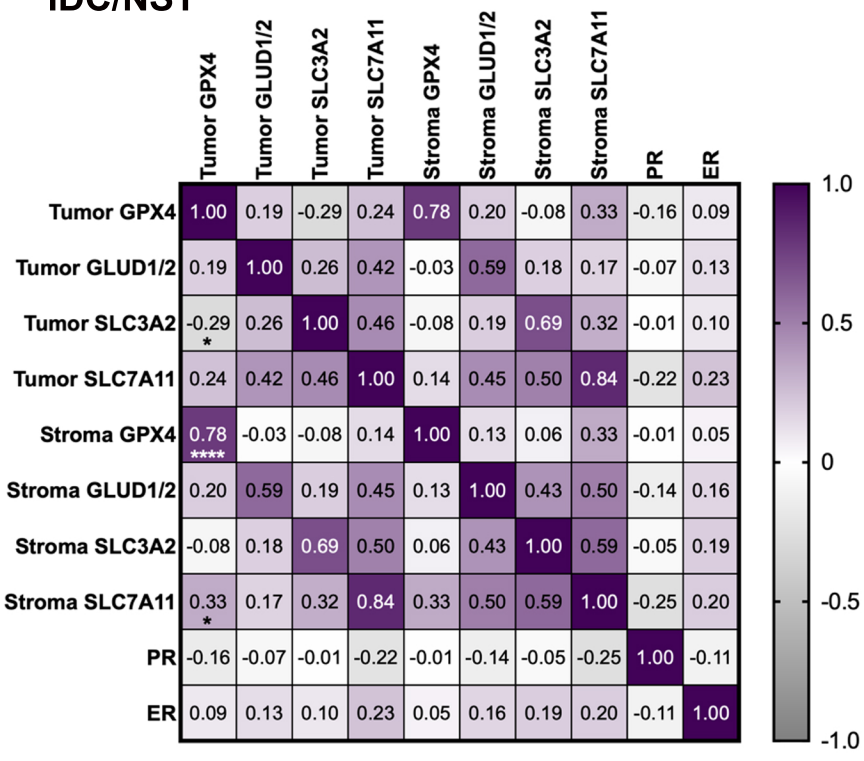

Figure 4. High GLUD1/2 expression is associated with increased tumor size and stage in Black women with ILC. A, Graphs illustrating the relationship between tumor size (cm) and percent positive cells for GPX4 and GLUD1/2 in Black women in the ILC cohort for panCK+ tumor cells. **B**, Spearman correlation coefficient (ρ) and p value for each protein's relationship to tumor size in panCK+ tumor cells and panCK- stromal cells for Black women in both the ILC and IDC/NST cohorts. **C**, *GLUD1* mRNA expression (RSEM, RNA-Seq by Expectation-Maximization) by tumor stage from TCGA for Black women with ILC (left) and Luminal A and Luminal B IDC/NST (right) breast cancer. Data are presented as a scatter plot, with the solid line indicating the median. *, *GLUD1* expression in Stage I vs Stage II Ductal breast cancer by unpaired t-test.

Figure 4

A.

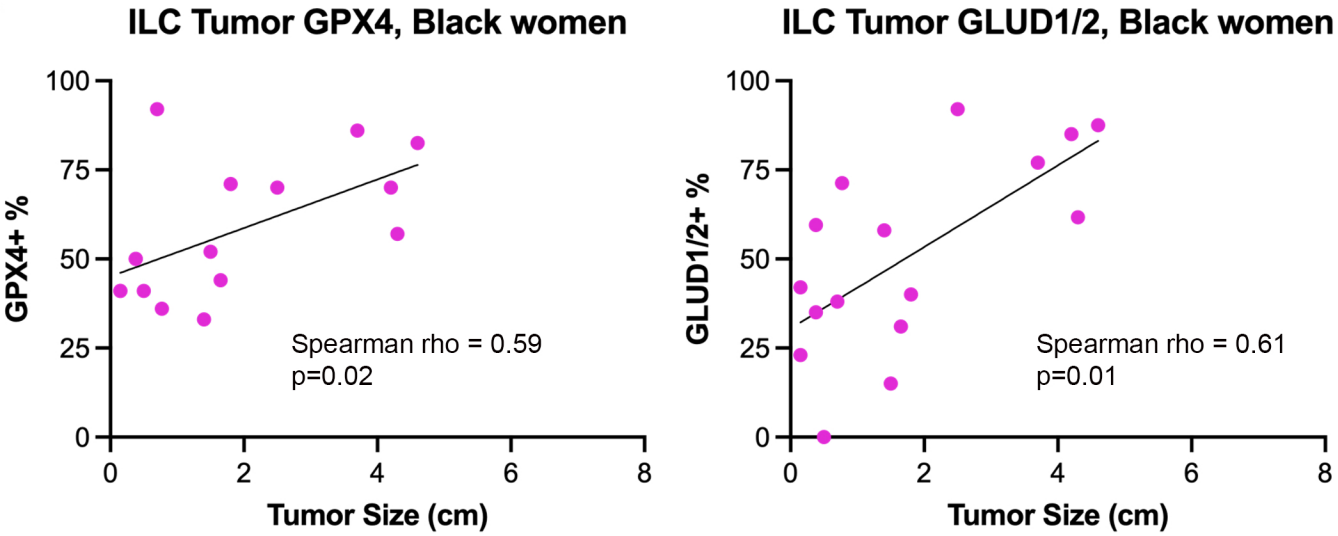

B.

Expression vs Tumor Size, Black women

Tumor				
Protein	**ILC Spearman ρ**	**ILC P Value**	**IDC/NST Spearman ρ**	**IDC/NST P Value**
GPX4	0.5873	0.0185*	-0.2953	0.2819
GLUD1/2	0.6097	0.0139*	-0.1650	0.5538
SLC3A2	0.5803	0.0204*	-0.2280	0.4102
SLC7A11	0.3729	0.1543	-0.3564	0.1906
Stroma				
Protein	**ILC Spearman ρ**	**ILC P Value**	**IDC/NST Spearman ρ**	**IDC/NST P Value**
GPX4	0.5729	0.0223*	-0.4272	0.1127
GLUD1/2	0.5940	0.0170*	-0.2083	0.4528
SLC3A2	0.5954	0.0167*	-0.5220	0.0481*
SLC7A11	0.3314	0.2087	-0.4789	0.0727

C.

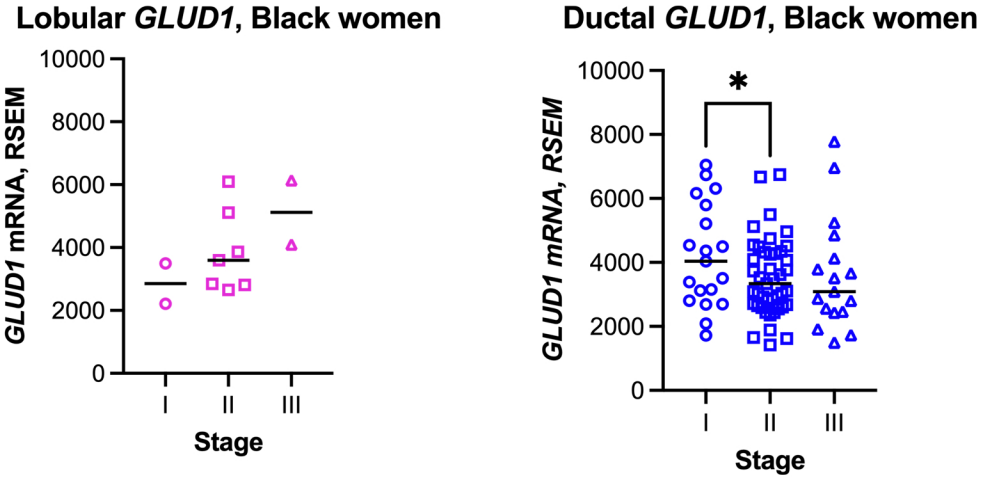

Figure 5. Enrichment of SLC3A2 and GPX4 in tumors from women with comorbidities in ILC and IDC/NST. A, Fisher's Exact Test of the presence or absence of any comorbidity, or specific comorbidities, in ILC compared to IDC/NST. **B**, Fisher's Exact Test of the presence or absence of any comorbidity in Black women compared to white women in the ILC and IDC/NST cohorts. **C**, Fisher's Exact Test of the proportion of high (above median) and low (below median) target expression in women with versus without comorbidity in the entire ILC (left, SLC3A2) and IDC/NST (right, GPX4) cohorts.

Figure 5

A.

Cohort Comorbidities					
	ILC		IDC/NST		P value
Comorbidity	Count	Percent	Count	Percent	
Any	19	26%	17	34%	0.421
Obesity	0	0%	7	14%	0.0015**
Hypertension	19	26%	1	2%	0.0003***

B.

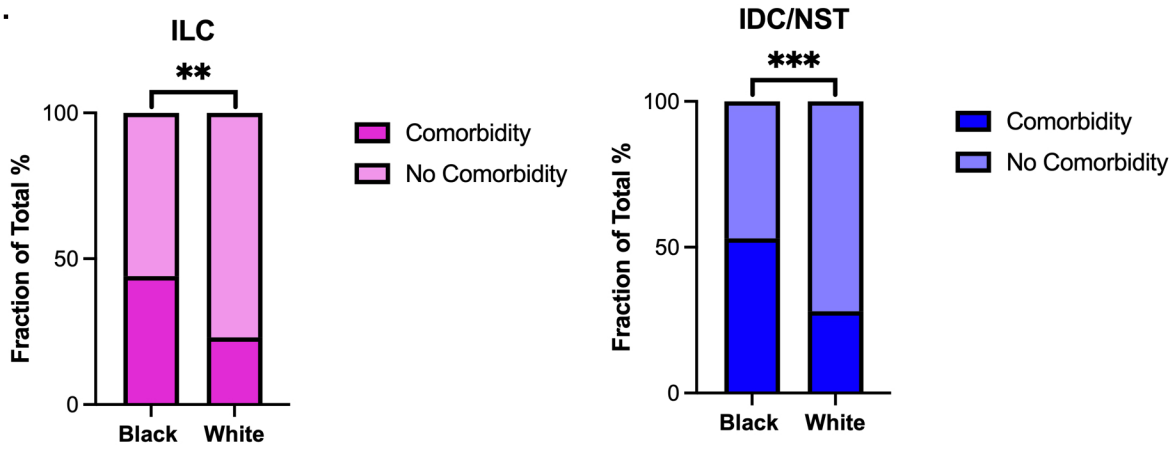

C.

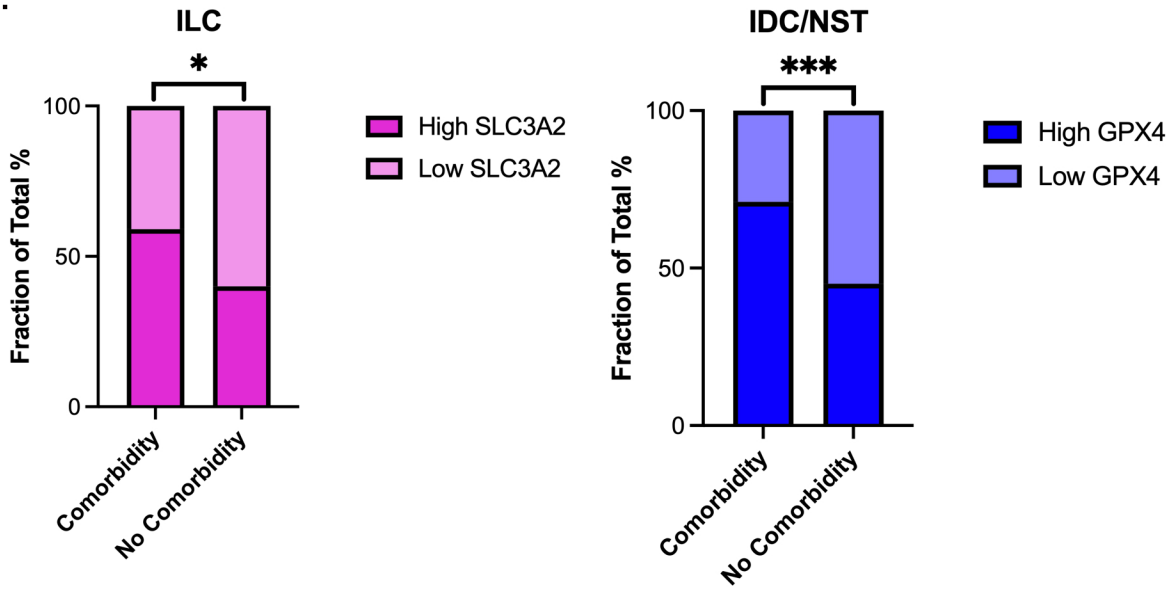

Figure 6. GLUD1 inhibition reduces ER protein levels, increases ROS, and reduces oxidative phosphorylation in endocrine therapy-resistant ILC cell lines. A, Heatmap of GLUD1 peptide count from ER RIME assays published by Sottnik et al[35]. Data are presented as the mean peptide count from two biological replicates of the SUM44, MM134, and BCK4 ILC cell lines. **B**, Immunoblot analysis of the expression of ER in ILC breast cancer cell lines cultured in the absence (-) and presence (+) of treatment with the GLUD1 inhibitor R162. Actin serves as a loading control. **C**, Flow cytometry analysis of SUM44 (left) and LCCTam cells (right) cultured in the absence (DMSO) and presence (R162) of the GLUD1 inhibitor, then stained with CellROX Deep Red and SYTOX Blue. Data from CellROX/SYTOX double-positive cells are normalized to the DMSO control, presented as the mean $\pm$ standard deviation for four independent experiments, and analyzed by Mann-Whitney U test. **D**, Metabolic imaging of NADH autofluorescence by fluorescence lifetime imaging (FLIM) and phasor analysis in LCCTam cells cultured in the absence (DMSO) and presence (R162) of the GLUD1 inhibitor. Oligomycin serves as a positive control to increase the proportion of free NADH by shifting cellular metabolism towards glycolysis. Upper panel shows a plot of normalized pixel number versus fractional intensity of free NADH (glycolysis) for treated and untreated cells. Lower panel shows representative images from one of eighteen independent fields of view for treated and untreated cells. Scale bar = 10 μm. Phasor – nuclear mask images are pseudo-colored based on the phasor plot (below) where more protein-bound and more free NADH phasor positions are indicated by red and green cursor circles, respectively. Pink/purple color represents increased protein-bound NADH (OXPHOS), and cyan indicates higher levels of free NADH (glycolysis).

Figure 6

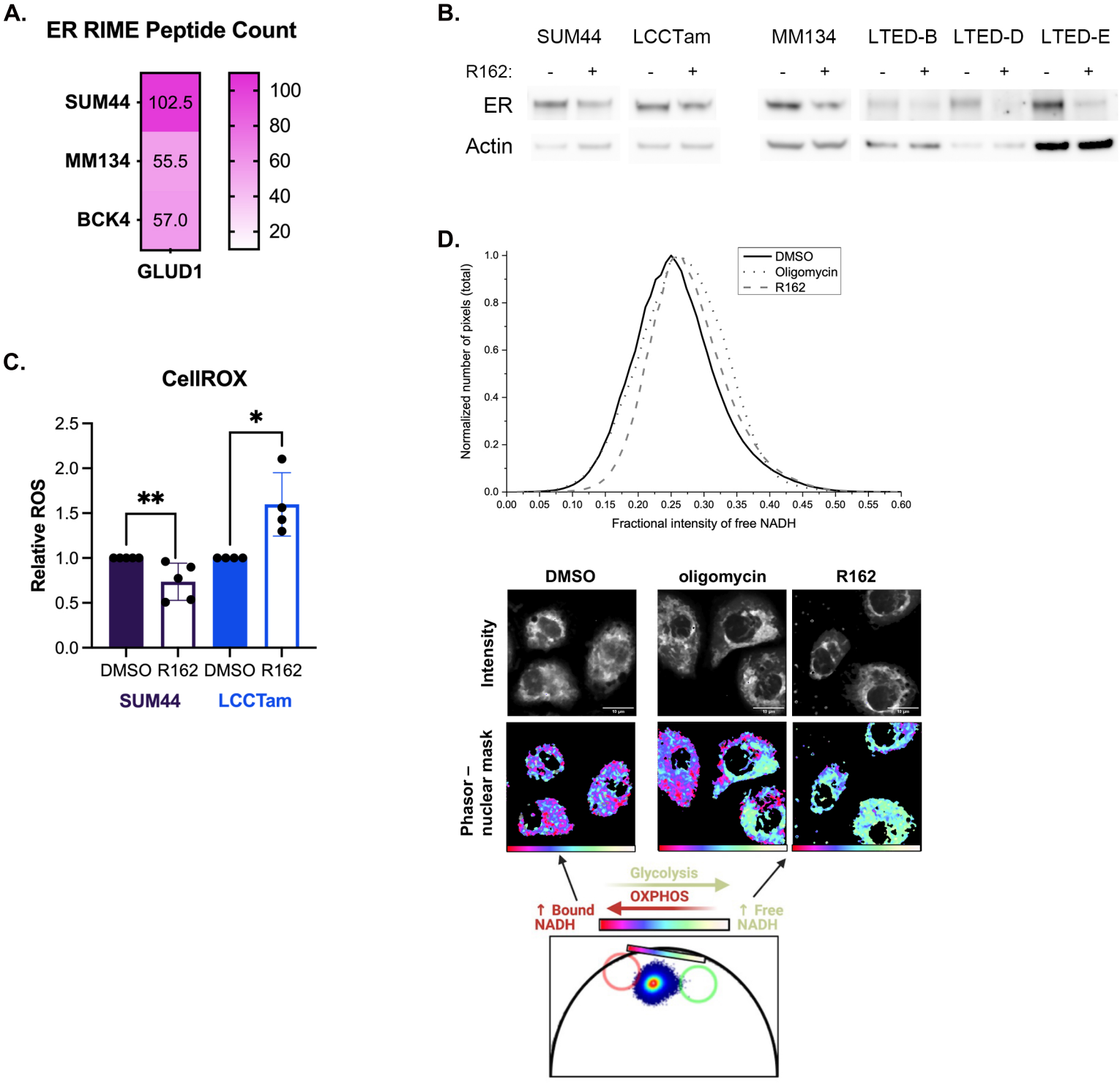

Supplemental Table 1: Primary Antibody/OPAL Dye Pairings and Incubation Conditions

	Antibody 1	Antibody 2	Antibody 3	Antibody 4	Antibody 5
Antigen	CD98	GLUD1/2	GPX4	panCK	SLC7A11
Company	Santa Cruz	Cell Signaling	Abcam	Agilent	Abcam
Cat#, RRID	Cat# sc-376815, RRID:AB_2938854	Cat# 12793, RRID:AB_2750880	Cat# ab125066, RRID:AB_10973901	Cat# M3515, RRID:AB_2132885	Cat# ab175186, RRID:AB_2722749
Species	Mouse	Rabbit	Rabbit	Mouse	Rabbit
Dilution	1:200	1:200	1:300	1:300	1:800
Incubation Time	1 hr	1 hr	1 hr	1 hr	1 hr
Incubation Temp.	RT	RT	RT	RT	RT
Control Tissue	Breast Cancer	Breast Cancer	Liver Cancer	Breast Cancer	Glioma
OPAL Fluor.	520	650	570	690	620
OPAL Conc.	1:150	1:150	1:400	1:30	1:300
Antigen Retrieval	AR6	AR6	AR6	AR6	AR6

Supplemental Table 2: Literature estimates of ILC prevalence in Black women

Author, Year (number of Black women)	Black and Lobular (%)	Significant vs NHW?	Reference
^Baquet, 2008 (nr)	nr (5.5%)	yes, ↓	50
Elledge, 1994 (1016)	nr	no	51
Gallagher, 2022 (295)	25 (8.5%)	yes, ↓	52
^Han, 2021 (7292)	541 (7.4%)	na	53
Oesterreich, 2022 (3022)	276 (7.6%)	yes, ↓	54
Williams, 2018 (1393)	126 (16%)	yes, ↓	55

n, number
NHW, non-Hispanic white
^Surveillance, Epidemiology, and End Results (SEER) data
nr, not reported
na, not applicable (Black women only)

Supplemental Table 3: Comorbidity Analysis
Two-sided Fisher's exact test was used for statistical analysis.

A) Overall comorbidity analysis for ILC and IDC/NST

	ILC	IDC	P-value
Comorbidity	19 (26.389%)	17 (34%)	0.4216 (NS)

- frequency and corresponding % represent the presence or absence of any comorbidity
- ILC: 9 out of 72 had multiple comorbidities
- IDC: 6 out of 50 had had multiple comorbidities

B) **Categorical comorbidity analysis for ILC and IDC/NST**

	ILC	IDC	P-value
Diabetes mellitus	5 (6.944%)	4 (8%)	>0.9999 (NS)
Hypercholesterolemia and/or hyperlipidemia	8 (11.111%)	1 (2%)	0.0804 (NS)
Obesity	0 (0%)	7 (14%)	0.0015 (**p<0.01)
Hypertension	19 (26.389%)	1 (2%)	0.0003 (***p<0.001)
Chronic kidney disease	0 (0%)	1 (2%)	0.4050 (NS)

Figure S1. **Expanded Data – Expression of glutamate-handling proteins in publicly available breast cancer datasets, and ILC cell lines. A**, Violin plots of mRNA expression data from invasive lobular breast cancer (ILC), mixed ductal-lobular breast cancer (mDLC), and breast cancer of no special type (NST) for each target in the multiplex IHC panel from TCGA, METABRIC, and SCAN-B. Data were analyzed and graphed using Gene Expression eXPLORER (GEXPLORER) at [35]. **B**, Left, immunoblot analysis of the expression of targets from the multiplex IHC panel in ILC breast cancer cell lines. SUM44 and LCCTam, pair of tamoxifen-sensitive and -resistant (respectively) cell lines. MM134 and LTED-A through E, series of parental (MM134) and long-term estrogen-deprived (LTED, mimicking aromatase inhibitor resistance) cell lines. Actin serves as a loading control. Right, graph showing fold change in expression (target:actin ratio) for each resistant cell line normalized to its parental control.

Figure S1

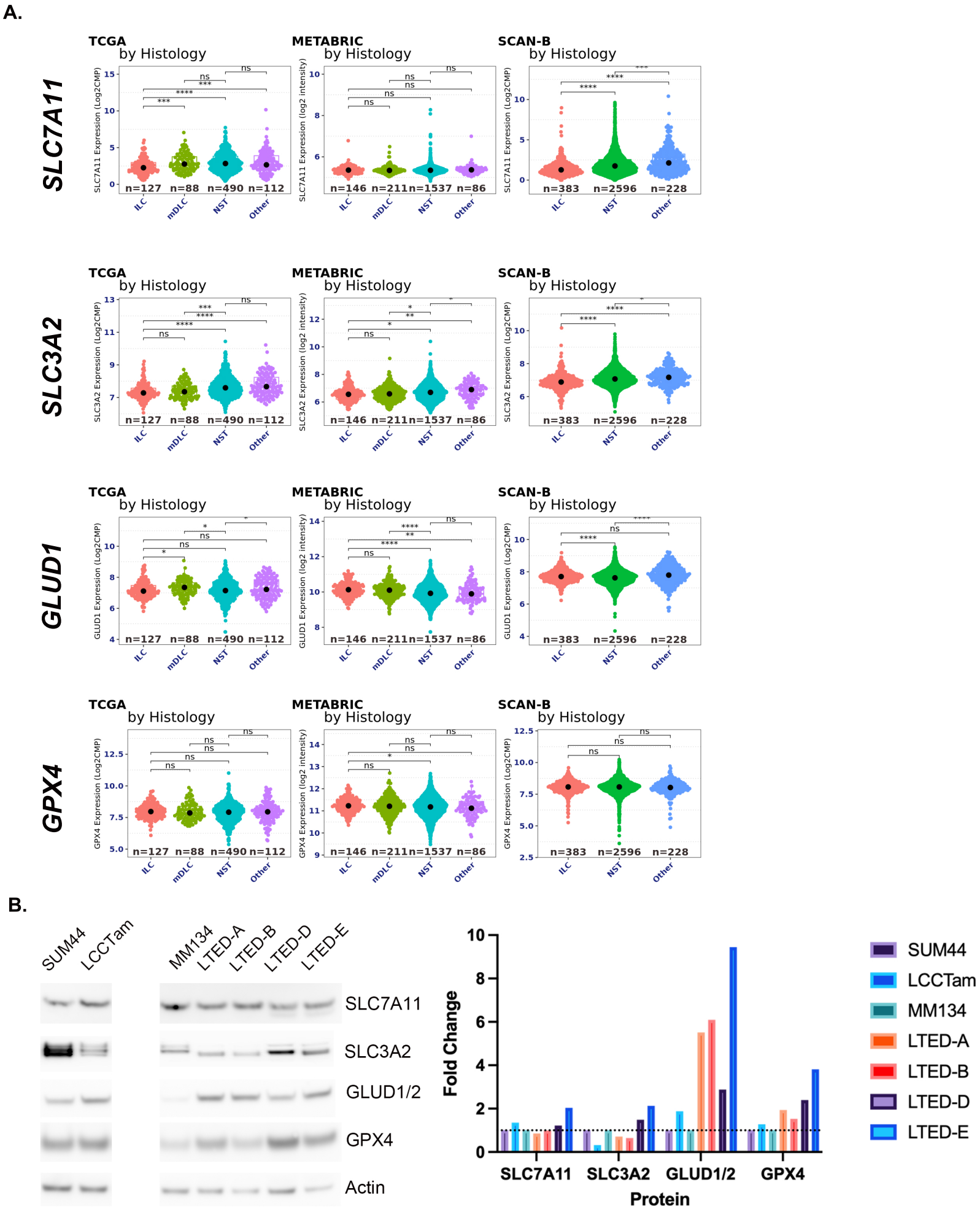

Figure S2. **Expanded Data – Expression of glutamate-handling proteins in ILC and IDC/NST**. Comparison of protein expression for SLC3A2 and SLC7A11 in the multiplex IHC panel between ILC and IDC/NST in panCK+ tumor cells (**A**) and panCK- stromal cells (**B**). Data are presented as a scatter plot, with each dot the mean of percent positive cells for an individual patient tumor and the solid line indicating the median. Data are analyzed by Mann-Whitney U test.

Figure S2